Ensconsin/Map7 promotes microtubule growth and centrosome separation in Drosophila neural stem cells.

Emmanuel Gallaud, Renaud Caous, Aude Pascal, Franck Bazile, Jean-Philippe Gagné, Sébastien Huet, Guy G Poirier, Denis Chrétien, Laurent Richard-Parpaillon, Régis Giet

Published March 31, 2014

Ensconsin/Map7 promotes microtubule growth and centrosome separation in *Drosophila* neural stem cells

Emmanuel Gallaud,[1] Renaud Caous,[1] Aude Pascal,[1] Franck Bazile,[2] Jean-Philippe Gagné,[4] Sébastien Huet,[3] Guy G. Poirier,[4] Denis Chrétien,[2] Laurent Richard-Parpaillon,[1] and Régis Giet[1]

[1]Cytoskeleton and Cell Proliferation, [2]Tubulin and Interacting Proteins, and [3]Spatio-temporal Regulation of Transcription, Biosit, Université de Rennes I, Centre National de la Recherche Scientifique, UMR 6290, 35043 Rennes, France
[4]Centre de Recherche du Centre Hospitalier Universitaire de Québec, Pavillon CHUL, Université Laval, Québec City, Québec G1V 0A6, Canada

The mitotic spindle is crucial to achieve segregation of sister chromatids. To identify new mitotic spindle assembly regulators, we isolated 855 microtubule-associated proteins (MAPs) from *Drosophila melanogaster* mitotic or interphasic embryos. Using RNAi, we screened 96 poorly characterized genes in the *Drosophila* central nervous system to establish their possible role during spindle assembly. We found that Ensconsin/MAP7 mutant neuroblasts display shorter metaphase spindles, a defect caused by a reduced microtubule polymerization rate and enhanced by centrosome ablation. In agreement with a direct effect in regulating spindle length, Ensconsin overexpression triggered an increase in spindle length in S2 cells, whereas purified Ensconsin stimulated microtubule polymerization in vitro. Interestingly, *ensc*-null mutant flies also display defective centrosome separation and positioning during interphase, a phenotype also detected in kinesin-1 mutants. Collectively, our results suggest that Ensconsin cooperates with its binding partner Kinesin-1 during interphase to trigger centrosome separation. In addition, Ensconsin promotes microtubule polymerization during mitosis to control spindle length independent of Kinesin-1.

Introduction

During mitosis, the mitotic spindle plays a crucial role in ensuring the correct segregation of chromosomes. One of the principal challenges faced by the cell during mitosis is the assembly of a powerful microtubule (Mt)-based machine mediating the efficient segregation of sister chromatids within a few minutes. Because of their role in defining the plane of cell division, mitotic Mts are also essential for brain homeostasis, a process linked to asymmetric stem cell division (Caussinus and Gonzalez, 2005; Wodarz and Näthke, 2007; Neumüller and Knoblich, 2009). The assembly of the spindle is complex and tightly regulated. The association of Mt-associated proteins (MAPs) with Mts and their subsequent dissociation play an essential role in mitotic spindle assembly. Mitotic spindle assembly and chromosome segregation thus require the complex spatial and temporal regulation of MAPs (Gadde and Heald, 2004).

Many MAPs have been identified in various model organisms. These proteins can be classified into two main categories: motor and nonmotor proteins. Through their direct effects on Mt dynamics, Mt sliding, and cross-linking, these MAPs are involved in several steps in mitosis: centrosome separation and positioning, the attachment of Mts to kinetochores (Kts), bipolar spindle formation, chromosome motion, and cytokinesis (Walczak and Heald, 2008). Mt polymerization is promoted by MAPs, such as TOGp/MAP215/msps (Cullen et al., 1999; Tournebize et al., 2000; Cassimeris and Morabito, 2004), and Mts are organized into a fusiform structure by motor proteins (Sawin et al., 1992; Wittmann et al., 1998; Goshima et al., 2005). Spindle size is controlled by the coordinated regulation of Mt end-binding proteins, such as CLASPs, depolymerizing

Correspondence to Régis Giet: regis.giet@univ-rennes1.fr

Abbreviations used in this paper: CNS, central nervous system; dsRNA, double-stranded RNA; EHR, Ensconsin homology region; GMC, ganglion mother cell; Khc, kinesin heavy chain; Kt, kinetochore; LC-MS/MS, liquid chromatography/tandem mass spectrometry; MAP, Mt-associated protein; Mt, microtubule; Nb, neuroblast; NEBD, nuclear envelope breakdown; SAC, spindle assembly checkpoint; WT, wild type.

Supplemental Material can be found at:
http://jcb.rupress.org/content/suppl/2014/03/27/jcb.201311094.DC1.html

The Rockefeller University Press $30.00
J. Cell Biol. Vol. 204 No. 7 1111–1121
www.jcb.org/cgi/doi/10.1083/jcb.201311094

Published March 31, 2014

kinesins, and the Mt minus end protein known as patronin (Gaetz and Kapoor, 2004; Maiato et al., 2004, 2005; Laycock et al., 2006; Goodwin and Vale, 2010).

This study focuses on Ensconsin/MAP7. We demonstrate, for the first time, the occurrence in *Drosophila melanogaster* neuroblasts (Nbs) of Ensconsin/MAP7-dependent interphase centrosome separation and spindle assembly pathways during mitosis.

Results and discussion

Ensconsin is a general MAP required for mitotic spindle assembly in the fly central nervous system (CNS)

We analyzed the *Drosophila* Mt interactome from 0–2-h-old embryos, which are characterized by rapid, synchronous cell divisions (mitotic embryos), with the goal of identifying new spindle assembly proteins. In parallel, we also investigated the Mt interactomes of older embryos (2–17 h old), in which most Mts have nonmitotic functions. Mt polymerization was induced by incubation with taxol, and the MAPs and Mts were harvested by centrifugation and resolved by SDS-PAGE (Fig. S1, A and B). We applied a high-throughput proteomics approach, leading to the high-confidence identification of 855 proteins in both samples (Fig. S1, C–E; and Table S2). Using spectral count, a semiquantitative measurement of protein abundance, we classified all the proteins identified as mitotic, general, or interphasic MAPs on the basis of their enrichment profiles (Materials and methods).

We investigated the possible role in spindle assembly in vivo of 96 poorly characterized genes by applying RNAi to the fly CNS (Table S3 and Fig. S1 F; Dietzl et al., 2007; Mummery-Widmer et al., 2009; Neumüller et al., 2011). The new putative mitotic genes identified by this approach (Fig. S1 G and Table S1) included *Ensconsin* (CG14998). We used *ensc* mutants to investigate the role of this gene in mitotic spindle assembly (Fig. 1 B, bottom). We used three known *Ensconsin* mutant alleles: *enscΔC* (C-terminal deletion), *enscΔN* (N-terminal deletion), and *enscΔNull* (full deletion, hereafter referred to as *ensc*; Sung et al., 2008). Western blot analyses showed all three mutant strains to have similar low levels of Ensconsin protein (see Fig. S3 A).

Ensc mutants had small brain lobes (Fig. 1 A) and a higher mitotic index (1.2 ± 0.5% in wild-type [WT] brains and 2.6 ± 1.0% in *ensc* mutant brains; $n > 3{,}000$ cells, 6 brains), which suggests that *ensc* mutation caused a mitotic delay due to prolonged spindle assembly checkpoint (SAC) activation. We tested this hypothesis with the double knockdown of Ensconsin and the SAC protein Mad2 by RNAi, with confirmation of the depletion of the protein (Fig. S2 A). Kt/Mt attachment defects were revealed by the large numbers of lagging chromatids during anaphase in double RNAi (6/30 anaphases) but not in cells subjected to *mad2* or *ensc* RNAi ($n > 40$ anaphases; Fig. S2, B and C). In addition, flies producing double-stranded RNAs (dsRNAs) for either *Ensconsin* or *Mad2* were viable, whereas flies producing both these RNAs died. This indicates that the SAC is required to prolong mitosis and to correct deleterious Kt–Mt attachment.

Ensconsin and Kinesin-1 mutant Nbs display similar centrosome separation defects during interphase

A close examination of *ensc* mutant Nb spindles revealed that the centrosomes were not fully separated at prophase (Fig. 1 B, top; $n = 20/91$) and that metaphase spindles were shorter than WT spindles (Fig. 1 B, bottom; $n > 300$ spindles).

Time-lapse imaging of dividing Nbs producing a GFP-tagged β-tubulin showed the time between nuclear envelope breakdown (NEBD) and anaphase onset to be 6.1 ± 0.9 min in WT cells and 8.0 ± 1.2 min in *ensc* mutants, which is consistent with SAC activation (Fig. 1, C and D, top; and Videos 1–3). We also confirmed that mean spindle length was significantly shorter in *ensc* mutants (8.2 ± 0.7 µm) than in the WT (10.7 ± 0.7; Fig. 1 D, bottom).

In *Drosophila* Nbs, unlike most cell types, the centrosomes split and start to separate immediately after cytokinesis (Rebollo et al., 2007; Rusan and Peifer, 2007). The daughter centrosome is immobile, retains Mt nucleation activity, and is connected to the apical cortex, whereas the mother centrosome displays weak Mt nucleation and migrates to the opposite side of the cell. The mother centrosome organizes a second aster shortly before mitosis. The daughter centrosome is therefore inherited by the Nb and the mother centrosome is inherited by the ganglion mother cell (GMC; Conduit and Raff, 2010; Januschke et al., 2011). The angle between the Mt asters before NEBD reflects the efficacy of centrosome separation. It was found to be abnormally low in *ensc* mutants (Fig. 1 E, top; and Fig. 1 F; see also Video 2), for which 14% of Nbs presented mispositioned asters during prophase (Fig. 1 E, bottom; and Video 3). The mother centrosome is not visible (by GFP-tubulin staining methods) before NEBD. We therefore imaged Nbs expressing YFP-labeled centrosomes and GFP-labeled Mts between two consecutive mitoses (Rebollo et al., 2007; Januschke and Gonzalez, 2010). Centrosome splitting after cytokinesis was normal in *ensc* mutants, but the separation was incomplete, resulting in the apparent separation defect detected before NEBD (Fig. 2 A, interphase; and Videos 4 and 5). We observed no monopolar spindle formation, which suggests that the machinery required to separate centrosomes at NEBD is functional (Tanenbaum and Medema, 2010). However, due to the late timing of separation, when the mother centrosome started to nucleate Mts at NEBD, it was often anchored to the apical cortex in place of the daughter centrosome and was therefore inherited by the Nb (8/25; Fig. 2 A and Video 5, green line).

Ensconsin is a coactivator of Kinesin-1 in interphase. We therefore investigated whether centrosome separation defects could be also detected after a loss of Kinesin-1 function (Sung et al., 2008; Metzger et al., 2012; Barlan et al., 2013). We found centrosome separation defects in khc^{27}/khc^{63} mutant brains, which lead to a small angle between centrosomes at NEBD but have no effect on spindle assembly (Fig. 2, B–E; and Videos 6 and 7). Centrosome inheritance was randomized and, in 50% of subsequent mitoses, the daughter centrosome ended up in the GMC (Fig. 2 D, bottom). These data demonstrate that early centrosome separation after cytokinesis is a prerequisite for correct centrosome segregation, a process in which Ensconsin and Kinesin-1

Published March 31, 2014

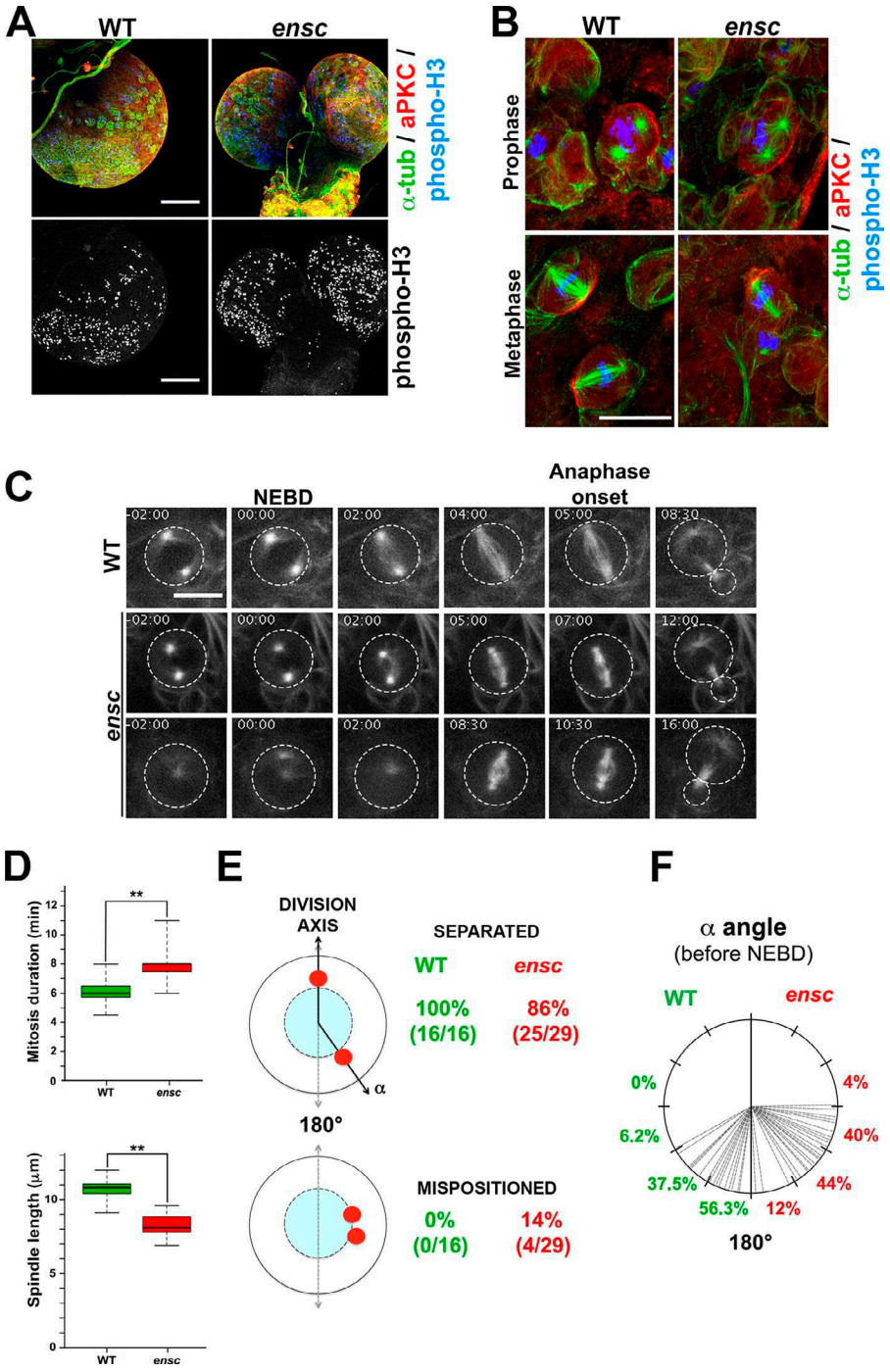

Figure 1. ***ensc* mutant Nbs display centrosome separation defects and shorter metaphase spindles.** (A) Overview of the optic lobes in WT and *ensc* mutant flies. *ensc* mutant larvae have small lobes and elevated numbers of mitotic cells. (B) Mitotic cells from WT or *ensc* mutant brains. A centrosome separation defect is detected in ∼15% of the *ensc* mutant prophase cells (top). *ensc* mutant metaphase spindles are shorter (bottom) than those in WT Nbs. aPKC is shown in red, tubulin in green, and phospho-histone H3 Ser10 in blue (gray in the bottom of A). Bars: (A) 100 µm; (B) 10 µm. (C) Dividing WT (top and Video 1) and *ensc* mutant (middle and bottom, and Videos 2 and 3) Nbs expressing β-tubulin–GFP. Note the mitotic delay in the *ensc* mutant, the shorter spindles, and the centrosome-positioning defect (bottom). Time is given in minutes:seconds. 00:00 corresponds to NEBD. The circles indicate the contours of the cells. Bar, 10 µm. (D) Analyses of the duration of mitosis (top) and spindle length (bottom) in WT (green) and *ensc* mutant (red) Nbs. Mitosis lasted 6.1 ± 0.9 min in the WT (n = 23) and 8.0 ± 1.2 min in the mutant (n = 37; **, P = 1.10 × 10^{-7}). Spindle length was 10.7 ± 0.7 µm in the WT (n = 15) and 8.2 ± 1.2 µm in *ensc* mutants (n = 23; **, P = 1.10 × 10^{-7}). (E) Analysis of centrosome separation in WT (green) and *ensc* mutant (red) Nbs at NEBD. 14% of *ensc* mutants display incomplete centrosome separation and severe mispositioning (Video 3). In the other cases (Video 2), the angle between the centrosomes relative to the center of the nucleus is measured (F). In WT, 93.8% of prophase cells have their basal centrosome oriented between 120° and 180°. In *ensc* mutants, only 56% of the cells position their centrosome in this region and 44% of the cells show an angle between 60° and 120°.

appear to be key players. Interestingly, spindle size and mitotic timing were normal in kinesin heavy chain (Khc)-depleted and mutant Nbs, which indicates a dependence of the short spindle phenotype on Ensconsin but not Kinesin-1 (Fig. 2 D).

Ensconsin is required for Mt growth in mitotic *Drosophila* Nbs

We analyzed the mitotic defects of the *ensc* mutants in detail by fully depolymerizing mitotic spindles from WT and *ensc* Nbs by cold treatment and monitoring Mt regrowth at 25°C (Fig. 3 A). In control tests, we observed large centrosomal asters 30 s after the return to 25°C conditions (Fig. 3 B, left, red arrows; n = 19). We also detected asters around the main chromosome mass and discrete Kt fibers (Fig. 3 B, white arrows). At 90 s, the WT spindles had a normal, bipolar shape (n = 25). The *ensc* mutant Nbs displayed weak aster formation around the chromosomes and no obvious Kt fibers after 30 s (n > 30; Fig. 3 B, right). After 90 s, only short spindles with weak, disorganized Mt arrays were present (n = 24). Overall, our results suggest that Ensconsin contributes to the polymerization of spindle Mts. For confirmation of this role, we quantified Mt growth directly by tracking EB1-GFP comets at Mt plus ends in WT and *ensc* Nbs (Fig. 3 C and Video 8). Measurements of Mt dynamic parameters revealed that the mean rate of Mt polymerization was significantly lower

Published March 31, 2014

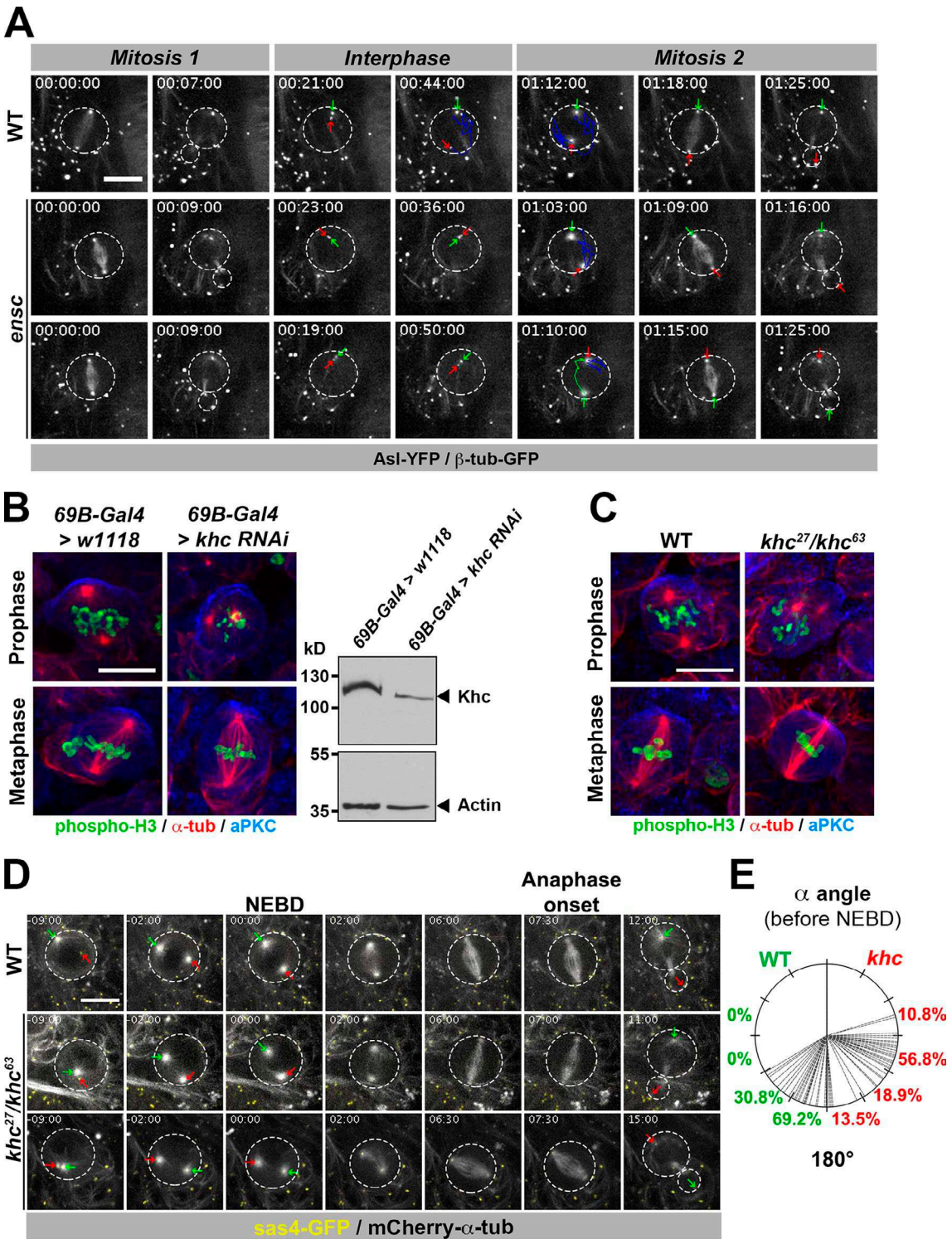

Figure 2. **Centrosome separation is defective in *kinesin-1* and *ensc* mutant Nbs.** (A) WT (top and Video 4) and *ensc* mutant (middle, bottom, and Video 5) Nbs expressing YFP-Asl (to label the centrosomes) and GFP-tubulin (to follow the daughter centrosome and Mts) were analyzed by time-lapse video microscopy. The green and blue lines follow the trajectories of the daughter and mother centrosomes, respectively. The two centrosomes did not separate fully in *ensc* mutants. For this reason, in several cases (8/25, 32%), when the mother centrosome acquired its Mt nucleation potential, it was attached to the apical cortex in place of the daughter centrosome, and was therefore inherited by the Nb rather than the GMC. (B) Prophase and metaphase in control or *khc* RNAi-treated Nbs (left) and Western blot analyses of Khc (top) and actin (bottom) after *khc* or control RNAi (right). (C) Prophase and metaphase in WT and khc^{27}/khc^{63} mutant Nbs. In B and C, tubulin is shown in red, aPKC in blue, and phospho-histone H3 Ser10 in green. (D) Duration of mitosis and centrosome positioning in WT and khc^{27}/khc^{63} mutant Nbs expressing Sas4-GFP (yellow) and Cherry-tubulin (gray). Mitosis lasted 7.2 ± 1.2 min in WT (n = 27) and 7.5 ± 1.5 min in khc^{27}/khc^{63} (n = 48) cells. P = 0.652. Spindle length was 10.9 ± 0.8 µm in WT cells and 11.3 ± 1.8 µm in khc^{27}/khc^{63} mutant cells. The daughter centrosome was inherited by the GMC in 24 of the 48 khc^{27}/khc^{63} mutant cells (50%). Time is given in hours:minutes:seconds. In A and D, the green and the red arrows indicate the daughter and mother centrosomes, respectively. The circles indicate the contours of the cells. Bars, 10 µm. (E) Analysis of centrosome separation angle in WT (green) and khc^{27}/khc^{63} (red) Nbs at NEBD.

Published March 31, 2014

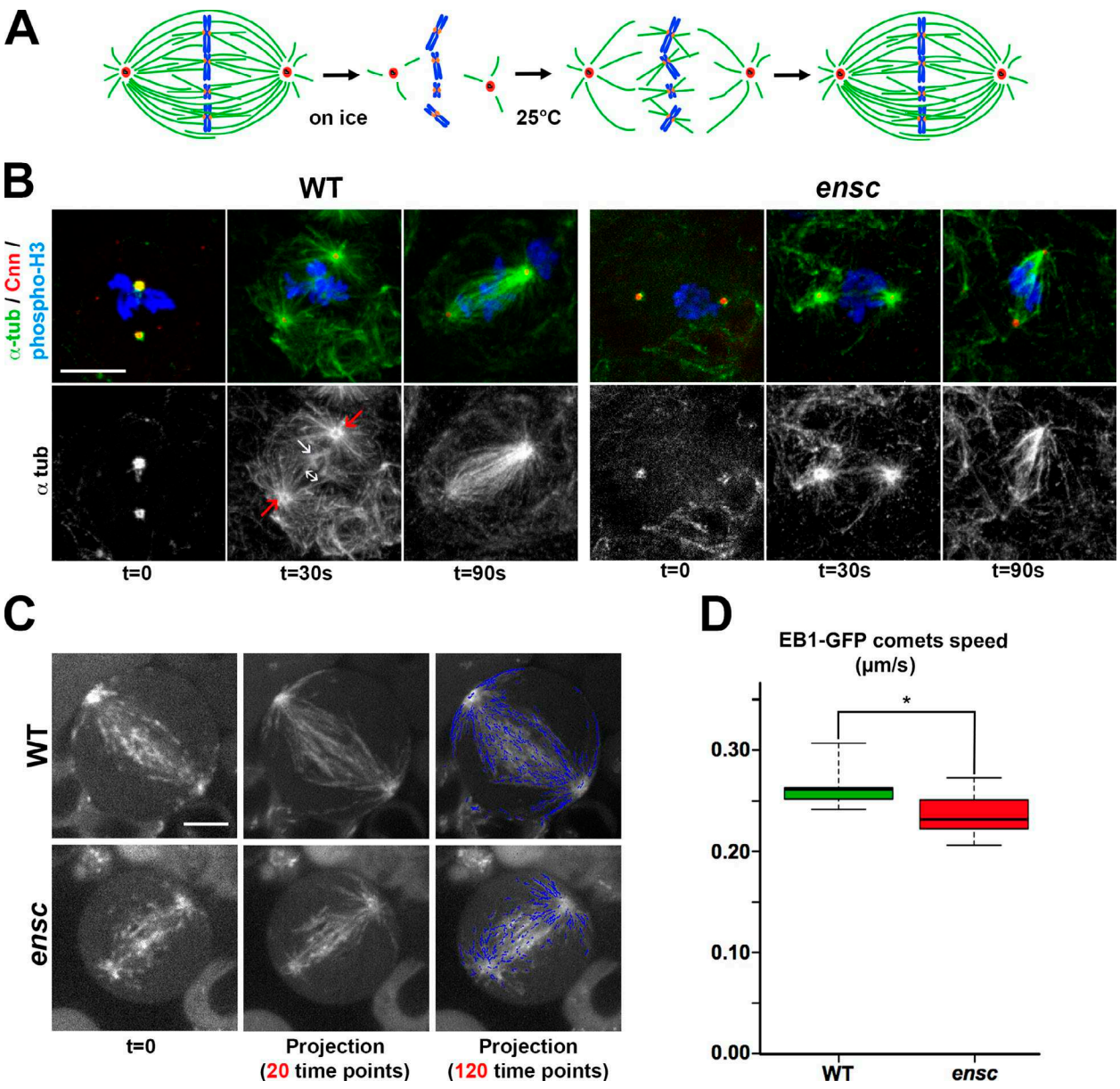

Figure 3. ***Ensconsin* mutant Nbs display defective spindle reassembly and a lower Mt velocity in live cells.** (A) Mt regrowth assay. Mts were depolymerized on ice (see Materials and methods), and spindle reformation was analyzed by immunostaining after the cells had been returned to 25°C conditions. (B) In the WT (left), Mts were depolymerized after 30 min at 0°C. Numerous Mts were nucleated by the centrosomes after 30 s at 25°C (red arrows). Small asters are visible around the chromatin (white arrow), together with Kt fibers (double-ended arrow). At 90 s, the spindles have a normal shape. In *ensc* mutant cells (right), only centrosomal Mts can be visualized after 30 s, and the spindles remain short and disorganized after 90 s. Centrosomes are shown in red (centrosomin, cnn), Mts (α tub) in green (gray in the lower panels), and phospho-H3 in blue. Bar, 10 µm. (C) Control (top) and *ensc* (bottom) Nbs expressing EB1-GFP were imaged by time-lapse microscopy (Video 8). A single frame (in which EB1-GFP comets are visible) is presented (left), with time projections for the 20- and 120-min time points (middle and right, respectively). Blue lines represent EB1-GFP tracks after filtering (see Materials and methods). Bar, 4 µm. (D) Quantification of Mt velocity in WT (n = 17) and *ensc* mutant (n = 16) mitotic Nbs: 0.26 and 0.23 µm/s, respectively (*, $P = 1.2 \times 10^{-4}$).

(reduced by 12%) in the *ensc* mutant than in WT Nbs (Fig. 3 D), a difference sufficient to account for the short spindles observed in *ensc* mutants.

Spindle shortening and the duration of mitosis in the Nbs of ensc mutants are greater in the absence of centrosomes

Given the large number of short Mts nucleated by the centrosomes in the regrowth assay, we investigated whether the spindle formation defects observed in *ensc* mutants were greater in the absence of centrosomes. We therefore generated *ensc* and *sas-4*^{s2214} double mutant flies, the *sas-4* gene being required for centrosome duplication (Basto et al., 2006), and monitored cell division (Fig. 4). In *sas-4*^{s2214} single mutants (Video 9, left), the spindle formed without centrosomes and mitosis lasted 9.0 ± 1.2 min (Fig. 4, A and C). In *ensc*,*sas-4*^{s2214} double mutants (Video 9, right), mitosis lasted significantly longer (10.1 ± 1.2 min) and the distribution of Mts was more strongly affected than in the single mutant (Fig. 4, A and C). The spindles were much shorter in the double mutant (6.7 ± 0.6 µm) than in the

Published March 31, 2014

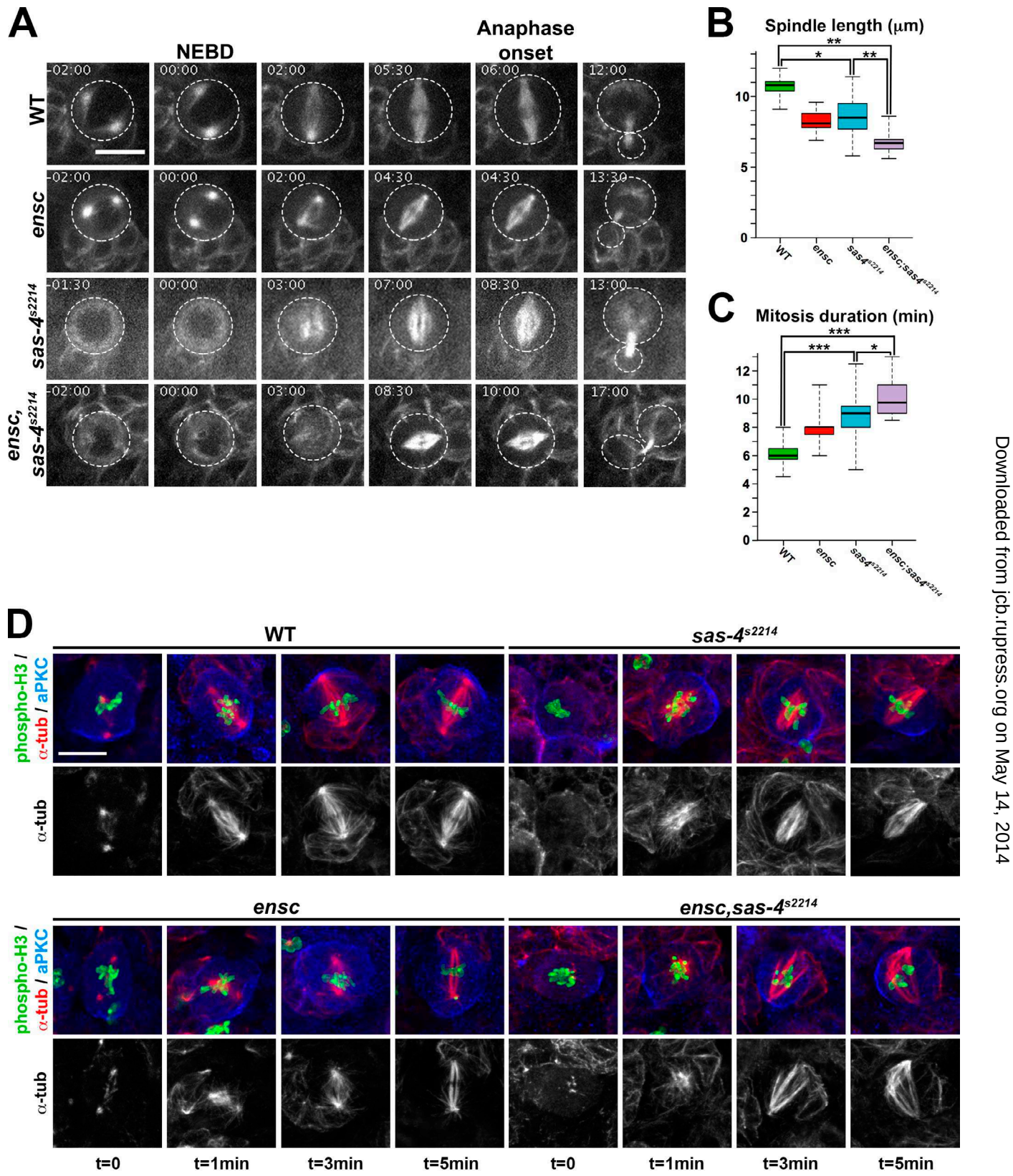

Figure 4. **Ensconsin-dependent spindle assembly defects are enhanced by centrosome ablation.** (A) Cell division of WT, *ensc*, *sas-4*^{s2214}, and *ensc*, *sas-4*^{s2214} double mutant Nbs expressing β-tubulin–GFP. Time is given in minutes:seconds. The circles indicate the contours of the cells. Bar, 10 µm. (B) Analysis of mitotic spindle length in WT (green), *ensc* (red), *sas-4*^{s2214} (blue), and *ensc,sas-4*^{s2214} (purple) mutant Nbs. Spindle length was 10.7 ± 0.7 µm in the WT (n = 15), 8.2 ± 1.2 µm in the *ensc* mutant (n = 23), 8.5 ± 1.4 µm in the *sas-4*^{s2214} mutant (n = 45), and 6.7 ± 0.7 µm in the *ensc,sas-4*^{s2214} double mutant (n = 31). *, P = 2 × 10^{-6}; **, P < 5.2 × 10^{-8}. (C) Analysis of the duration of mitosis in WT (green), *ensc* (red), *sas-4*^{s2214} (blue), and *ensc,sas-4*^{s2214} (purple) mutant Nbs. The time between NEBD and anaphase onset was 6.1 ± 0.9 min for the controls (n = 23), 8.0 ± 1.2 min for the *ensc* mutant (n = 37), 9.0 ± 1.2 min for the *sas-4*^{s2214} mutant (n = 48), and 10.0 ± 1.2 min for the *ensc,sas-4*^{s2214} double mutant (n = 38). *, P = 1.8 × 10^{-3}; ***, P < 1 × 10^{-10}.

Published March 31, 2014

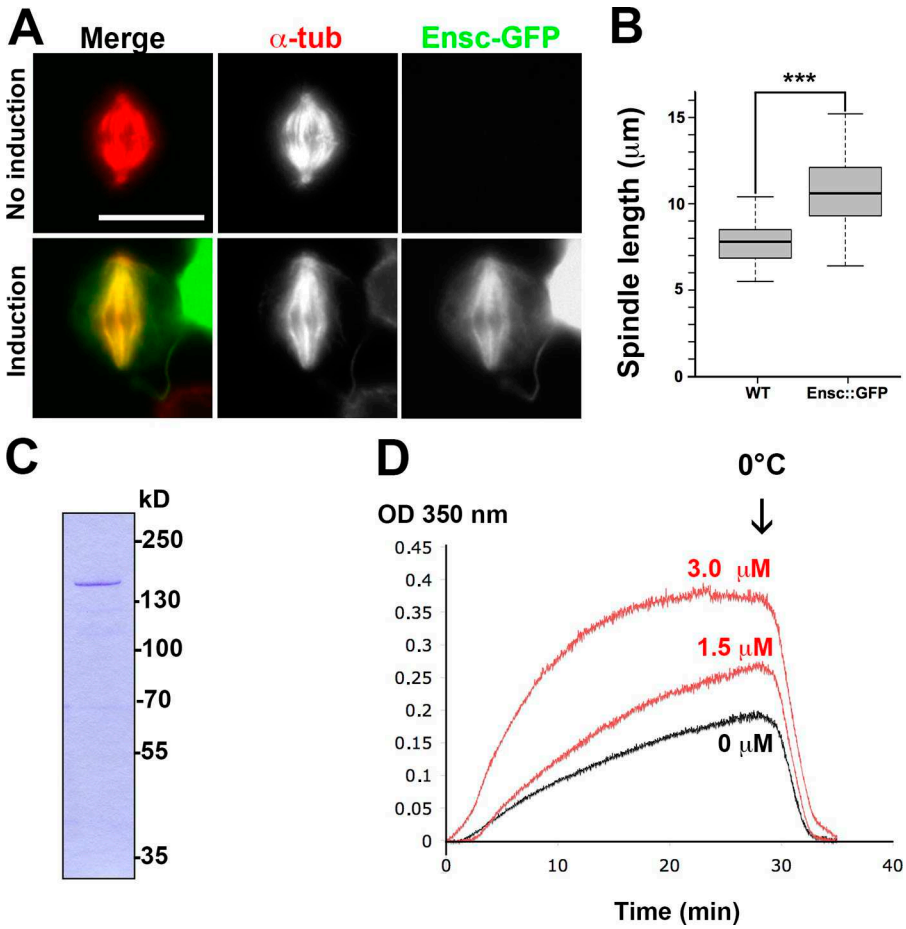

Figure 5. **Ensconsin promotes Mt growth in cells and in vitro.** (A) Ensconsin (Ensc) overproduction in mitotic S2 cells led to the formation of longer spindles. Ensconsin-GFP is green (gray in the panels on the right) and Mts are shown in red (gray in the middle panels). Exogenous Ensconsin-GFP is localized on the mitotic spindle during mitosis. Bar, 10 μm. (B) Analysis of mitotic spindle length in WT (n = 56) and Ensconsin-GFP–overexpressing mitotic S2 cells (n = 26). ***, $P = 5.1 \times 10^{-11}$. (C) Recombinant Ensconsin purified, separated by SDS-PAGE, and stained with Coomassie blue. (D) Effect of Ensconsin on Mt polymerization in vitro. Purified porcine brain tubulin was mixed with polymerization buffer supplemented with either PBS or PBS containing Ensconsin on ice. Mt polymerization was induced by heating at 35°C. Absorbance at 350 nm was monitored to evaluate the formation of Mt polymers. After 28 min, the samples were shifted to 0°C to estimate protein aggregation. Ensconsin increased the rate of Mt polymerization and the total number of polymers in a dose-dependent manner (red curves), as shown by comparison with buffer alone (black curve).

sas-4^{s2214} (8.5 ± 1.4 μm) and *ensc* single mutants (8.0 ± 0.6 μm; Fig. 4 B). In parallel, we repeated the Mt regrowth assay (Fig. 4 D). 1 min after the return to 25°C, long Mts were seen in the WT and the *sas-4*^{s2214} single mutant, but not in the *ensc* single mutant and the *ensc*,*sas-4*^{s2214} double mutant. Bipolar spindle assembly occurred within 3 min in flies lacking either *sas-4*^{s2214} or *ensconsin*, but was severely compromised in the double mutant. These results suggest that the centrosome favors spindle assembly when Mt polymerization rates are low in mitotic *ensc* mutant cells.

Ensconsin is a mitotic spindle-associated protein that stimulates Mt growth in S2 cells and in vitro

We analyzed the distribution of Ensconsin by staining dividing *Drosophila* embryos with purified antibodies. Ensconsin colocalized with the mitotic apparatus during early development (Fig. S3 B). Furthermore, studies of a functional *Drosophila* line ubiquitously expressing the GFP-tagged Ensconsin confirmed the colocalization of Ensconsin-GFP with the Mt network and the mitotic spindle during Nb cell division and in early embryos (Fig. S3, C and D; and Video 10).

Consistent with the Ensconsin-dependent stimulation of Mt growth during M phase, S2 cells with higher Ensconsin levels formed longer spindles (10.9 ± 2.1 μm, n = 26) than control cells (7.8 ± 1.0 μm, n = 56; Fig. 5, A and B). In a complementary experiment, we assessed the impact of Ensconsin activity on Mt polymerization in vitro, using purified porcine brain tubulin and recombinant Ensconsin (Fig. 5 C) in a turbidity assay, to determine whether this protein could modify the Mt polymerization rate in vitro (Weis et al., 2010; Gaskin, 2011). Ensconsin stimulated Mt polymerization in a dose-dependent manner (Fig. 5 D). This function is entirely consistent with a lower Mt velocity in the deletion mutant and with a longer spindle length in conditions of Ensconsin overexpression.

In conclusion, our study reveals a dual role for Ensconsin. First, during interphase, this protein promotes centrosome separation and positioning through cooperation with its binding partner, Kinesin-1. Second, it stimulates Mt growth during mitosis, independent of Kinesin-1.

(D) Mt regrowth assay in WT, *ensc*, *sas-4*^{s2214}, and *ensc*,*sas-4*^{s2214} mutant Nbs. 1 and 3 min after the return to 25°C, numerous long Mts were detected in *sas-4*^{s2214} Nbs. In the *ensc*,*sas-4*^{s2214} double mutant, short Mts were found closely apposed to the mitotic chromatin mass. At 5 min, the spindles resembled Mt bundles rather than the bipolar structure seen in *sas-4*^{s2214} mutants. aPKC is shown in blue, Mts (α-tub) are shown in red (and gray), and phospho-H3 is shown is green. Bar, 10 μm.

Published March 31, 2014

Human Ensconsin/MAP7/EMAP115 was first discovered two decades ago, and was described as a MAP that "ensconces" on Mts (Bulinski and Bossler, 1994). The data presented here reveal previously unidentified roles for this known MAP in the regulation of mitotic and interphase Mt–based processes. Further studies are required to determine how a single MAP can contribute to such different activities during the cell cycle.

Materials and methods

Mt co-sedimentation assay

Canton-S fly populations were amplified, maintained, and fed in population cages with fresh yeast on agar plates twice daily for 5 d. We collected 0–2-h-synchronized embryos, a time period corresponding to syncytial division. In parallel, flies were allowed to lay eggs for 15 h and the collected embryos were left for an additional 2 h to allow the last embryos laid to reach the blastula stage. This protocol discriminates between the dividing/mitotic and differentiating/interphase stages. We disrupted 1 g of mitotic and interphase embryos by passage through a French press in a total volume of 2 ml of lysis buffer (LB: 20 mM Hepes, pH 7.4,150 mM KCl, 1 mM $MgCl_2$, 1 mM EDTA, and 0.5% NP-40) supplemented with protease inhibitor and phosphatase inhibitor cocktails, prepared according to the manufacturer's instructions (Roche). The crude extracts were filtered and centrifuged for 15 min at 15,000 *g*. The resulting supernatant (~1.2 ml) was centrifuged at 100,000 *g* for 25 min at 4°C to remove insoluble materials. These mitotic and interphase supernatants, obtained by high-speed centrifugation, were supplemented with 1 mM GTP and 20 µM taxol, and incubated for 20 min at 25°C. The polymerized Mts and MAPs were then recovered by centrifugation for 20 min at 100,000 *g* and 25°C on a glycerol cushion (BRB80: 80 mM Pipes, 1 mM EGTA supplemented with 40% glycerol, 1 mM GTP, and 20 µM taxol). The Mt pellets were washed gently twice with BRB80 and suspended in Laemmli sample buffer supplemented with 5% β-mercaptoethanol.

Liquid chromatography/tandem mass spectrometry (LC-MS/MS)

MAPs were resolved by SDS-PAGE in 4–12% XT Bis-Tris polyacrylamide gradient gels (Bio-Rad Laboratories). The gel was stained with SYPRO Ruby gel stain according to the manufacturer's instructions (Bio-Rad Laboratories). A Geliance charge-coupled device (CCD)–based imaging system (PerkinElmer) was used for image acquisition.

The lanes on the SDS-PAGE gel corresponding to mitotic and interphase/differentiating embryo extracts were cut into 20 gel slices per lane with a disposable lane picker (Gel Company). Gel slices were deposited in 96-well plates. A liquid handling station (MassPrep; Waters) was used, with sequencing-grade modified trypsin (Promega) according to the manufacturer's instructions, for in-gel protein digestion. Peptide extracts were then dried by evaporation in a SpeedVac (Thermo Fisher Scientific).

LC-MS/MS experiments were performed with an LTQ linear ion trap mass spectrometer connected to a Thermo Surveyor MS pump and equipped with a nanoelectrospray ion source (all from Thermo Fisher Scientific). The peptides were separated in a 10-cm-long PicoFrit BioBasic C18 column with an internal diameter of 0.075 mm (New Objective), with a linear gradient extending from 2 to 50% solvent B (acetonitrile, 0.1% formic acid) over a period of 30 min, at a flow rate of 200 nl/min. Mass spectra were acquired in the data-dependent acquisition mode (Xcalibur software, version 2.0). Each full-scan mass spectrum (m/z 400–2000) was followed by the collision-induced dissociation of the seven ions giving the most intense signals. The dynamic exclusion function was enabled (30 s of exclusion), and the relative collisional fragmentation energy was set at 35%.

All MS/MS spectra were analyzed with Mascot (version 2.4.0; Matrix Science), set up to search against a *Drosophila* UniRef100 protein database (33,950 entries as of November 2012), assuming digestion with trypsin. The fragment and parent ion mass tolerances were 0.5 D and 2.0 D, respectively. The carbamidomethylation of cysteine was specified as a fixed modification, and the oxidation of methionine and phosphorylation on serine, threonine, and tyrosine were specified as variable modifications. Two missed cleavages were allowed.

Scaffold (version 3.6.2; Proteome Software, Inc.) was used to sum spectral counts, to validate MS/MS-based peptide and protein identifications, and to group peptides into proteins. Peptide identifications were accepted if they could be established with a probability >95%, as specified by the Peptide Prophet algorithm (Nesvizhskii et al., 2003), and contained at least two identified peptides. Protein probabilities were assigned by the Protein Prophet algorithm (Keller et al., 2002). Proteins that contained similar peptides and could not be differentiated on the basis of MS/MS analysis alone were grouped to satisfy the principles of parsimony. Semiquantitative spectral count analysis results obtained with Scaffold provide an estimate of relative protein abundance between conditions. Enrichment ratios were calculated from spectral count information for interphase extracts.

Functional enrichment analysis and network analysis

We used Cytoscape 2.8.3 and BiNGO version 2.44 to identify biological processes overrepresented among the proteins classified into mitotic, general, or interphasic MAPs (Shannon et al., 2003; Maere et al., 2005). We used BiNGO with the GO Slim Generic Gene Ontology Annotation. The significance threshold was set at P = 0.05 (hypergeometric test, Benjamini and Hochberg family-wise error rate correction).

Plasmid constructs

All constructs were based on isoform B of Ensconsin, which has been shown to rescue *ensc* mutants (Sung et al., 2008). All cloning procedures were performed with the Gateway system (Life Technologies) and the clones were checked by sequencing. Full-length Ensconsin, the N-terminal Mt-binding domain/Ensconsin homology region 1 domain (MBD/EHR1), and the conserved C-terminal EHR2 domain were amplified by PCR and inserted into the pENTR/TOPO vector (Life Technologies) to create the entry clones from PCR products: full-length Ensconsin (Ensc-FL), without a STOP codon, with the primers 5′-CACCAATATGGCGAGTCTTGGGGGCCAACAC-3′ and 5′-CAGCAGCGATATATCTTTATTTTCGTGAC-3′; an N-terminal fragment containing the EHR1 domain (Ensc-EHR1), with the primers 5′-CACCAATATGGCGAGTCTTGGGGGCCAACAC-3′ and 5′-CGGAGGTTCCCGCTTCGAAGGCGTCTTC-3′; and a C-terminal fragment containing the EHR2 fragment (Ensc-EHR2), with the primers 5′-CACCATGCAGGCTGCGCCCAAGAAACCATCGC-3′ and 5′-CAGCAGCGATATATCTTTATTTTCGTGAC-3′.

Ensc-FL, Ensc-EHR1, and Ensc-EHR2 were also inserted into pET102/TOPO (Life Technologies) to generate hexahistidine (6X-HIS)-tagged constructs. Ensc-EHR1 and Ensc-EHR2 were also recombined in pMT-DEST48. Ensc-FL-GFP was amplified by PCR with the primers 5′-GCAATGGCGAGTCTTGGGG-3′ and 5′-AATCTTGTACAGCTCGTCCATGC-3′ and inserted directly into pMT/V5-His-TOPO.

Isoform E of EB1 was amplified by PCR with the oligonucleotides 5′-CACCAACATGGCTGTAAACGTCTACTCC-3′ and 5′-ATACTCCTCGTCCTCTGGTGG-3′ and inserted into pENTR/TOPO.

The open reading frames encoding EB1 and Ensconsin were introduced into pUWG with Gateway technology (Invitrogen) to produce the constructs pUWG-EB1 and pUWG-Ensc used for fly transformation, allowing the ubiquitous expression of GFP-tagged proteins.

Fly strains

Flies were maintained under standard conditions at 25°C. Transgenic flies with the following genotypes were used for RNAi: TubGAL80^{ts};69B-GAL4 and 69B-GAL4. Transgenic flies carrying UAS and hairpin sequences were obtained from the Vienna *Drosophila* RNAi Center (Dietzl et al., 2007). Flies expressing the full-length EB1-GFP and full-length Ensconsin-GFP constructs were used for time-lapse imaging. They were obtained from BestGene Inc. after P-element–mediated transformation with the pUWG-EB1 and pUWG-Ensc vectors. The Ensconsin-GFP transgene conferred early rescue of the viability of *ensc* mutants. Asterless-YFP (Asl)-expressing flies (Rebollo et al., 2007) were provided by C. Gonzalez (Institute for Research in Biomedicine, Barcelona, Spain). *Khc* mutant flies carrying amino-acid substitutions have been described elsewhere (Djagaeva et al., 2012) and were provided by A. Guichet (Institut Jacques Monod, Paris, France), B. Saxton (University of California, Santa Cruz, Santa Cruz, CA), and A. Ephrussi (European Molecular Biology Laboratory, Heidelberg, Germany). A combination of Khc^{27} (null allele) and Khc^{63} (hypomorphic allele) was used in this study. The strains expressing mCherry–α-tubulin and GFP-Sas-4 were provided by R. Basto (Institut Curie, Paris, France) and M. Bettencourt-Dias (Instituto Gulbenkian de Ciencia, Oeiras, Portugal), respectively. The *ensconsin* mutant fly stocks *enscΔC* (C-terminal deletion), *enscΔN* (N-terminal deletion), and *enscΔnull* (full gene deletion, referred to as *ensc*) were described in the Results and discussion section, obtained by P-element excision, and were provided by P. Rorth (Institute of Molecular and Cell Biology, Singapore; Sung et al., 2008). β-tubulin–GFP flies (Inoue et al., 2004) were provided by M. Savoian and D. Glover (University of Cambridge, Cambridge, England, UK). Jupiter-GFP and the *sas-4^{s2214}* mutant (Basto et al., 2006) were obtained from the Bloomington Drosophila

Published March 31, 2014

Stock Center. With the exception of Jupiter-GFP, which is a trap line with expression under the control of its own promoter (Morin et al., 2001), all GFP and CherryFP fusion proteins were ubiquitously produced under the control of the polyubiquitin promoter.

RNAi in the brain

TUB-GAL80^{ts}; 69B-GAL4 females were crossed with transgenic males carrying UAS-RNAi constructs for the candidate genes. After 6 d at 20°C, the adults were removed and the vials were shifted to 29°C to induce RNAi for 3 d. Brains from five wandering third-instar larvae were then dissected and fixed for immunostaining. In parallel, at least five brains were squashed and stained with 1 µg/ml DAPI for the visualization of chromosome abnormalities (Donaldson et al., 2001).

Production of recombinant proteins and antibody

The vectors pET102-Ensc-FL, pET102-Ensc-EHR1, and pET102-Ensc-EHR2 were transformed in *Escherichia coli* BL21 (DE3). The production of the Ensc-FL, Ensc-EHR1, and Ensc-EHR2 fragments was induced by incubation with 1 mM IPTG for 4 h at 25°C. 6×-HIS–tagged proteins were purified on Ni-NTA resin (QIAGEN) and dialyzed overnight against PBS at 4°C. The purified Ensconsin EHR1 and EHR2 domains present in all Ensconsin isoforms were generally used for the immunization of rabbits for polyclonal antibody production (Eurogentec). For in vitro Mt polymerization assays, Ensc-FL was concentrated on Amicon concentrators (molecular weight cut-off 50 kD) to a final concentration of 30 µM in PBS (EMD Millipore).

Immunofluorescence analysis

S2 cells were plated on concanavalin A–coated coverslips and incubated for 1 h, then fixed by incubation in methanol for 10 min at −20°C. The fixed cells were processed for IF analyses as described previously (Romé et al., 2010). Slides were mounted in ProLong Gold antifading mounting medium (Life Technologies) and observed under an upright DMRXA fluorescence microscope (Leica) equipped with a 63× 1.3 NA objective lens. Images were acquired with a CCD camera (CoolSNAP HQ; Photometrics) and processed with MetaMorph software (Universal Imaging).

For the analysis of spindle morphology in brain Nbs, we found that the following protocol fully preserved the Mt cytoskeleton during mitosis more effectively than the use of the standard PBS-derived fixative. For whole-mount CNS immunostaining, third-instar larval brains were dissected in testis buffer (TB: 183 mM KCl, 47 mM NaCl, 10 mM Tris, and 1 mM EDTA, pH 6.8; Bonaccorsi et al., 2011) and fixed by incubation in TBF (TB supplemented with 10% formaldehyde and 0.01% Triton X-100) for 20 min at 25°C.

Fixed brains were rapidly washed once in PBS and twice in 0.1% Triton X-100 in PBS (PBST) for 10 min each time. The fixed tissue was incubated overnight at 4°C with primary antibodies in PBST supplemented with 1% BSA (PBSTB). The samples were washed twice, for 15 min each time, in PBST, and were then incubated for 1 h at room temperature with secondary antibodies in PBSTB. They were washed twice, for 15 min each time, in PBST, then mounted on slides in ProLong Gold and observed with a SP5 confocal microscope (Leica) equipped with a 63× objective lens (NA 1.40). Images were acquired and processed with ImageJ software.

For the Mt regrowth assay in Nbs, we followed a method previously used to study *misato*, with several modifications (Mottier-Pavie et al., 2011). Brains were dissected in Schneider's medium supplemented with 10% FCS and incubated on ice for 30 min to allow complete Mt depolymerization in a total volume of 50 µl of Schneider's medium. Depending on the genotype analyzed, Mt regrowth was induced at various time points by incubating the samples in a water bath at 25°C. Fixation is triggered by adding 500 µl of TBF and incubating for 20 min at 25°C. Brains were then processed for immunostaining. The experiment was performed at least three times and at least 20 spindles were analyzed for each experiment.

Antibodies and Western blotting

The monoclonal YL1/2 rat anti-detyrosinated tubulin antibody (1:200) and the mouse monoclonal and rabbit polyclonal antiphosphorylated histone H3 (Ser10) antibodies (1:500) were obtained from EMD Millipore. The anti-GFP mouse monoclonal antibody (1:1,000) was obtained from Roche, the rabbit anti-PKCζ (C-20; 1:200) and rabbit anti-actin (1:4,000) polyclonal antibodies were obtained from Santa Cruz Biotechnology, Inc., the mouse monoclonal anti-V5 antibody was obtained from Life Technologies (1:3,000), and the rabbit polyclonal anti-Khc antibody (1:2,000) was obtained from Cytoskeleton, Inc. The rabbit polyclonal anti-centrosomin antibody (1:1,000) was provided by T. Megraw (Florida State University, Tallahassee, FL; Megraw et al., 2001). The affinity-purified rabbit anti-Mad2 polyclonal antibody (1:500) was provided by D. Sharp (Albert Einstein College of Medicine, Bronx, NY). The rabbit polyclonal anti-Ensconsin antibody was affinity purified from antigens (EH1 and EH2) immobilized on nitrocellulose membrane and used at a concentration of 1 µg/ml according to a protocol described previously (Montembault et al., 2007). Goat secondary peroxidase-conjugated antibodies (1:5,000) were obtained from Jackson ImmunoResearch Laboratories, and donkey Alexa Fluor–conjugated secondary antibodies (1:1,000) were obtained from Life Technologies. For Western blotting, ECL reagent was purchased from Thermo Fisher Scientific.

Live microscopy

Brains expressing the various labeled proteins were dissected in Schneider's *Drosophila* medium containing 10% FCS. Isolated brains were loaded and mounted on stainless steel slides with fat bodies dissected from WT larvae (Siller et al., 2005). The preparations were sealed with mineral oil (Sigma-Aldrich). Images were acquired with a spinning-disk system mounted on an inverted microscope (Eclipse Ti; Nikon) equipped with a 60× 1.4 NA objective lens at 25°C. Z series were acquired every 30 or 60 s with a CCD camera (CoolSNAP HQ^2; Photometrics) and a digital camera (sCMOS ORCA Flash 4.0; Hamamatsu Photonics) controlled by MetaMorph acquisition software version X. Images were processed with ImageJ software and are presented as maximum-intensity projections. The mother and daughter centrosomes can be unambiguously distinguished on the basis of their different Mt nucleation potentials after separation, after cytokinesis, or immediately before mitosis (Rebollo et al., 2007).

For Mt end tracking in Nbs, WT and *ensc* mutant brains expressing EB1-GFP were gently squashed in 13.4 µl of fresh Schneider's media (Invitrogen), between a slide and a 22 × 22-mm coverslip, and the excess medium was absorbed with filter paper. The preparation was sealed with mineral halocarbon oil 700 (Sigma-Aldrich) to immobilize it and to prevent cell movement during imaging. Mitotic Nbs were imaged every 0.5 s for 1 min at 25°C, with a 100× 1.4 NA objective lens.

At least 16 mitotic prometaphase Nbs were imaged for comet tracking.

The Mt ends were tracked with the single-particle tracking routine available in Icy image analysis software (Olivo-Marin, 2002; Chenouard et al., 2013). The routine parameters were adjusted for the detection and tracking of most of the Mt ends. Nevertheless, because of the high density of Mts, we observed frequent erroneous merging of tracks corresponding to different Mt ends. These errors were filtered out with a customized Matlab (MathWorks) routine. The crude tracks were first broken at track steps characterized by an instantaneous speed of >0.78 µm/s, probably corresponding to erroneous jumps between different Mt tracks. They were also broken at positions at which a change in track direction of >60° was observed. We retained only the remaining filtered tracks corresponding to at least three time points and we estimated the growing speed for each track by averaging the instantaneous speeds along the track.

Cell culture and transfection

S2 cells were transiently transfected as described previously, and protein production was induced by incubation with 0.3 mM $CuSO_4$ for 24 h (Romé et al., 2010).

Mt self-assembly and turbidity assays

A 40-µM solution of tubulin purified from porcine brain was prepared in 1 mM GTP in BRB80, and centrifuged for 10 min at 30,000 *g*, at 4°C, before assembly (Weis et al., 2010). Tubulin polymerization was induced by incubating the samples at 35°C and was monitored turbidimetrically, at 350 nm, with a UVIKON XS spectrophotometer (BioTek Instruments). We evaluated Ensconsin activity by adding various concentrations of the recombinant protein to tubulin (1.5 and 3 µM). For each experiment, the temperature was shifted to 4°C after 28 min of recording to estimate the degree of protein aggregation after assembly (Weis et al., 2010). Spectrophotometric curves were corrected so as to reflect only Mt polymerization.

Statistical analysis

Differences between datasets were assessed in a nonparametric test (Mann-Whitney-Wilcoxon), with values of $P < 0.001$ considered significant.

Online supplemental material

Fig. S1 shows the screening strategy used in this study. Fig. S2 demonstrates that the SAC is required for viability and to prevent chromosome segregation defects after *Ensc* RNAi. Fig. S3 shows the specificity of the Ensconsin antibody and Ensconsin localization. Table S1 summarizes the phenotypes obtained after RNAi for 18 putative mitotic regulators. Table S2

shows the proteins associated with mitotic and interphase Mt pellets, respectively, and their relative abundance. Table S3 shows the proteins screened in this study. Video 1 shows WT dividing Nbs. Video 2 shows dividing *ensc* mutant Nbs with short spindles. Video 3 shows *ensc* dividing Nbs with centrosome positioning and separation defects. Video 4 shows a WT Nb, expressing labeled centrosomes and Mts, between two consecutive mitoses. Video 5 shows the centrosome separation defects in an *ensc* mutant during interphase and the defective daughter centrosome inheritance. Video 6 shows the centrosomes and the Mts in a WT Nb. Video 7 demonstrates the defective centrosome separation, positioning, and inheritance defect but normal spindle assembly in *khc* mutants. Video 8 shows the Mt dynamics in WT and *ensc* mitotic Nbs. Video 9 shows the short spindle formation in the absence of centrosome and in the absence of both centrosome and Ensconsin. Video 10 reveals the Ensconsin-GFP fusion protein association with Mts in a dividing Nb and surrounding cells. Supplemental file 1, entitled "trajfilt," corresponds to the source code of the routine used to filter the trajectories of the Mt ends obtained from the single particle tracking routine available on the Icy image analysis software. Supplemental file 2, entitled "trajfilt_batch," corresponds to the source code of the routine which allows batching the filtering of the Mt end trajectories. Online supplemental material is available at http://www.jcb.org/cgi/content/full/jcb.201311094/DC1.

We would like to thank D. Glover, M. Savoian, C. Gonzalez, T. Megraw, D. Sharp, D. Buster, A. Guichet, W. Saxton, R. Basto, A. Ephrussi, M. Bettencourt-Dias, and P. Rorth for fly stocks and antibodies. We thank M. Savoian, C. Benaud, and S. Giet for critical reading of the manuscript. We thank Drs. A. Royou and E. Montembault for helpful discussions.

This work was funded by the Ligue Nationale Contre le Cancer, l'Association de la Recherche contre le Cancer, Biosit, and the University of Rennes 1. This work was supported by the Canadian Institutes of Health Research (grant No. MO-178013 to GGP). The authors wish to thank the Proteomics Platform of Quebec Genomic Center for analytical services and the Microscopy Rennes Imaging Center. G.G. Poirier holds a Canada Research Chair in Proteomics. E. Gallaud and R. Caous are doctoral fellows of the Région Bretagne and the French Ministry of Research, respectively.

The authors declare no competing financial interests.

Submitted: 21 November 2013
Accepted: 12 February 2014

References

Barlan, K., W. Lu, and V.I. Gelfand. 2013. The microtubule-binding protein ensconsin is an essential cofactor of kinesin-1. *Curr. Biol.* 23:317–322. http://dx.doi.org/10.1016/j.cub.2013.01.008

Basto, R., J. Lau, T. Vinogradova, A. Gardiol, C.G. Woods, A. Khodjakov, and J.W. Raff. 2006. Flies without centrioles. *Cell*. 125:1375–1386. http://dx.doi.org/10.1016/j.cell.2006.05.025

Bonaccorsi, S., M.G. Giansanti, G. Cenci, and M. Gatti. 2011. Preparation of meiotic chromosomes from larval and pupal *Drosophila* testes. *Cold Spring Harb Protoc*. 2011:t5579.

Bulinski, J.C., and A. Bossler. 1994. Purification and characterization of ensconsin, a novel microtubule stabilizing protein. *J. Cell Sci.* 107:2839–2849.

Cassimeris, L., and J. Morabito. 2004. TOGp, the human homolog of XMAP215/Dis1, is required for centrosome integrity, spindle pole organization, and bipolar spindle assembly. *Mol. Biol. Cell*. 15:1580–1590. http://dx.doi.org/10.1091/mbc.E03-07-0544

Caussinus, E., and C. Gonzalez. 2005. Induction of tumor growth by altered stem-cell asymmetric division in *Drosophila melanogaster*. *Nat. Genet.* 37:1125–1129. http://dx.doi.org/10.1038/ng1632

Chenouard, N., I. Bloch, and J.C. Olivo-Marin. 2013. Multiple hypothesis tracking for cluttered biological image sequences. *IEEE Trans. Pattern Anal. Mach. Intell.* 35:2736–3750. http://dx.doi.org/10.1109/TPAMI.2013.97

Conduit, P.T., and J.W. Raff. 2010. Cnn dynamics drive centrosome size asymmetry to ensure daughter centriole retention in *Drosophila* neuroblasts. *Curr. Biol.* 20:2187–2192. http://dx.doi.org/10.1016/j.cub.2010.11.055

Cullen, C.F., P. Deák, D.M. Glover, and H. Ohkura. 1999. mini spindles: A gene encoding a conserved microtubule-associated protein required for the integrity of the mitotic spindle in *Drosophila*. *J. Cell Biol.* 146:1005–1018. http://dx.doi.org/10.1083/jcb.146.5.1005

Dietzl, G., D. Chen, F. Schnorrer, K.C. Su, Y. Barinova, M. Fellner, B. Gasser, K. Kinsey, S. Oppel, S. Scheiblauer, et al. 2007. A genome-wide transgenic RNAi library for conditional gene inactivation in *Drosophila*. *Nature*. 448:151–156. http://dx.doi.org/10.1038/nature05954

Djagaeva, I., D.J. Rose, A. Lim, C.E. Venter, K.M. Brendza, P. Moua, and W.M. Saxton. 2012. Three routes to suppression of the neurodegenerative phenotypes caused by kinesin heavy chain mutations. *Genetics*. 192:173–183. http://dx.doi.org/10.1534/genetics.112.140798

Donaldson, M.M., A.A. Tavares, H. Ohkura, P. Deak, and D.M. Glover. 2001. Metaphase arrest with centromere separation in polo mutants of *Drosophila*. *J. Cell Biol.* 153:663–676. http://dx.doi.org/10.1083/jcb.153.4.663

Gadde, S., and R. Heald. 2004. Mechanisms and molecules of the mitotic spindle. *Curr. Biol.* 14:R797–R805. http://dx.doi.org/10.1016/j.cub.2004.09.021

Gaetz, J., and T.M. Kapoor. 2004. Dynein/dynactin regulate metaphase spindle length by targeting depolymerizing activities to spindle poles. *J. Cell Biol.* 166:465–471. http://dx.doi.org/10.1083/jcb.200404015

Gaskin, F. 2011. Analysis of microtubule assembly kinetics using turbidimetry. *Methods Mol. Biol.* 777:99–105. http://dx.doi.org/10.1007/978-1-61779-252-6_7

Goodwin, S.S., and R.D. Vale. 2010. Patronin regulates the microtubule network by protecting microtubule minus ends. *Cell*. 143:263–274. http://dx.doi.org/10.1016/j.cell.2010.09.022

Goshima, G., R. Wollman, N. Stuurman, J.M. Scholey, and R.D. Vale. 2005. Length control of the metaphase spindle. *Curr. Biol.* 15:1979–1988. http://dx.doi.org/10.1016/j.cub.2005.09.054

Inoue, Y.H., M.S. Savoian, T. Suzuki, E. Máthé, M.T. Yamamoto, and D.M. Glover. 2004. Mutations in orbit/mast reveal that the central spindle is comprised of two microtubule populations, those that initiate cleavage and those that propagate furrow ingression. *J. Cell Biol.* 166:49–60. http://dx.doi.org/10.1083/jcb.200402052

Januschke, J., and C. Gonzalez. 2010. The interphase microtubule aster is a determinant of asymmetric division orientation in *Drosophila* neuroblasts. *J. Cell Biol.* 188:693–706. http://dx.doi.org/10.1083/jcb.200905024

Januschke, J., S. Llamazares, J. Reina, and C. Gonzalez. 2011. *Drosophila* neuroblasts retain the daughter centrosome. *Nat Commun*. 2:243. http://dx.doi.org/10.1038/ncomms1245

Keller, A., A.I. Nesvizhskii, E. Kolker, and R. Aebersold. 2002. Empirical statistical model to estimate the accuracy of peptide identifications made by MS/MS and database search. *Anal. Chem.* 74:5383–5392. http://dx.doi.org/10.1021/ac025747h

Laycock, J.E., M.S. Savoian, and D.M. Glover. 2006. Antagonistic activities of Klp10A and Orbit regulate spindle length, bipolarity and function in vivo. *J. Cell Sci.* 119:2354–2361. http://dx.doi.org/10.1242/jcs.02957

Maere, S., K. Heymans, and M. Kuiper. 2005. BiNGO: a Cytoscape plugin to assess overrepresentation of gene ontology categories in biological networks. *Bioinformatics*. 21:3448–3449. http://dx.doi.org/10.1093/bioinformatics/bti551

Maiato, H., C.L. Rieder, and A. Khodjakov. 2004. Kinetochore-driven formation of kinetochore fibers contributes to spindle assembly during animal mitosis. *J. Cell Biol.* 167:831–840. http://dx.doi.org/10.1083/jcb.200407090

Maiato, H., A. Khodjakov, and C.L. Rieder. 2005. *Drosophila* CLASP is required for the incorporation of microtubule subunits into fluxing kinetochore fibres. *Nat. Cell Biol.* 7:42–47. http://dx.doi.org/10.1038/ncb1207

Megraw, T.L., L.R. Kao, and T.C. Kaufman. 2001. Zygotic development without functional mitotic centrosomes. *Curr. Biol.* 11:116–120. http://dx.doi.org/10.1016/S0960-9822(01)00017-3

Metzger, T., V. Gache, M. Xu, B. Cadot, E.S. Folker, B.E. Richardson, E.R. Gomes, and M.K. Baylies. 2012. MAP and kinesin-dependent nuclear positioning is required for skeletal muscle function. *Nature*. 484:120–124. http://dx.doi.org/10.1038/nature10914

Montembault, E., S. Dutertre, C. Prigent, and R. Giet. 2007. PRP4 is a spindle assembly checkpoint protein required for MPS1, MAD1, and MAD2 localization to the kinetochores. *J. Cell Biol.* 179:601–609. http://dx.doi.org/10.1083/jcb.200703133

Morin, X., R. Daneman, M. Zavortink, and W. Chia. 2001. A protein trap strategy to detect GFP-tagged proteins expressed from their endogenous loci in *Drosophila*. *Proc. Natl. Acad. Sci. USA*. 98:15050–15055. http://dx.doi.org/10.1073/pnas.261408198

Mottier-Pavie, V., G. Cenci, F. Vernì, M. Gatti, and S. Bonaccorsi. 2011. Phenotypic analysis of misato function reveals roles of noncentrosomal microtubules in *Drosophila* spindle formation. *J. Cell Sci.* 124:706–717. http://dx.doi.org/10.1242/jcs.072348

Mummery-Widmer, J.L., M. Yamazaki, T. Stoeger, M. Novatchkova, S. Bhalerao, D. Chen, G. Dietzl, B.J. Dickson, and J.A. Knoblich. 2009. Genome-wide analysis of Notch signalling in *Drosophila* by transgenic RNAi. *Nature*. 458:987–992. http://dx.doi.org/10.1038/nature07936

Nesvizhskii, A.I., A. Keller, E. Kolker, and R. Aebersold. 2003. A statistical model for identifying proteins by tandem mass spectrometry. *Anal. Chem.* 75:4646–4658. http://dx.doi.org/10.1021/ac0341261

Neumüller, R.A., and J.A. Knoblich. 2009. Dividing cellular asymmetry: asymmetric cell division and its implications for stem cells and cancer. *Genes Dev.* 23:2675–2699. http://dx.doi.org/10.1101/gad.1850809

Neumüller, R.A., C. Richter, A. Fischer, M. Novatchkova, K.G. Neumüller, and J.A. Knoblich. 2011. Genome-wide analysis of self-renewal in *Drosophila* neural stem cells by transgenic RNAi. *Cell Stem Cell*. 8:580–593. http://dx.doi.org/10.1016/j.stem.2011.02.022

Olivo-Marin, J.C. 2002. Extraction of spots in biological images using multiscale products. *Pattern Recognit.* 35:1989–1996. http://dx.doi.org/10.1016/S0031-3203(01)00127-3

Rebollo, E., P. Sampaio, J. Januschke, S. Llamazares, H. Varmark, and C. González. 2007. Functionally unequal centrosomes drive spindle orientation in asymmetrically dividing *Drosophila* neural stem cells. *Dev. Cell*. 12:467–474. http://dx.doi.org/10.1016/j.devcel.2007.01.021

Romé, P., E. Montembault, N. Franck, A. Pascal, D.M. Glover, and R. Giet. 2010. Aurora A contributes to p150(glued) phosphorylation and function during mitosis. *J. Cell Biol.* 189:651–659. http://dx.doi.org/10.1083/jcb.201001144

Rusan, N.M., and M. Peifer. 2007. A role for a novel centrosome cycle in asymmetric cell division. *J. Cell Biol.* 177:13–20. http://dx.doi.org/10.1083/jcb.200612140

Sawin, K.E., K. LeGuellec, M. Philippe, and T.J. Mitchison. 1992. Mitotic spindle organization by a plus-end-directed microtubule motor. *Nature*. 359:540–543. http://dx.doi.org/10.1038/359540a0

Shannon, P., A. Markiel, O. Ozier, N.S. Baliga, J.T. Wang, D. Ramage, N. Amin, B. Schwikowski, and T. Ideker. 2003. Cytoscape: a software environment for integrated models of biomolecular interaction networks. *Genome Res.* 13:2498–2504. http://dx.doi.org/10.1101/gr.1239303

Siller, K.H., M. Serr, R. Steward, T.S. Hays, and C.Q. Doe. 2005. Live imaging of *Drosophila* brain neuroblasts reveals a role for Lis1/dynactin in spindle assembly and mitotic checkpoint control. *Mol. Biol. Cell*. 16:5127–5140. http://dx.doi.org/10.1091/mbc.E05-04-0338

Sung, H.H., I.A. Telley, P. Papadaki, A. Ephrussi, T. Surrey, and P. Rørth. 2008. *Drosophila* ensconsin promotes productive recruitment of Kinesin-1 to microtubules. *Dev. Cell*. 15:866–876. http://dx.doi.org/10.1016/j.devcel.2008.10.006

Tanenbaum, M.E., and R.H. Medema. 2010. Mechanisms of centrosome separation and bipolar spindle assembly. *Dev. Cell*. 19:797–806. http://dx.doi.org/10.1016/j.devcel.2010.11.011

Tournebize, R., A. Popov, K. Kinoshita, A.J. Ashford, S. Rybina, A. Pozniakovsky, T.U. Mayer, C.E. Walczak, E. Karsenti, and A.A. Hyman. 2000. Control of microtubule dynamics by the antagonistic activities of XMAP215 and XKCM1 in Xenopus egg extracts. *Nat. Cell Biol.* 2:13–19.

Walczak, C.E., and R. Heald. 2008. Mechanisms of mitotic spindle assembly and function. *Int. Rev. Cytol.* 265:111–158. http://dx.doi.org/10.1016/S0074-7696(07)65003-7

Weis, F., L. Moullintraffort, C. Heichette, D. Chrétien, and C. Garnier. 2010. The 90-kDa heat shock protein Hsp90 protects tubulin against thermal denaturation. *J. Biol. Chem.* 285:9525–9534. http://dx.doi.org/10.1074/jbc.M109.096586

Wittmann, T., H. Boleti, C. Antony, E. Karsenti, and I. Vernos. 1998. Localization of the kinesin-like protein Xklp2 to spindle poles requires a leucine zipper, a microtubule-associated protein, and dynein. *J. Cell Biol.* 143:673–685. http://dx.doi.org/10.1083/jcb.143.3.673

Wodarz, A., and I. Näthke. 2007. Cell polarity in development and cancer. *Nat. Cell Biol.* 9:1016–1024. http://dx.doi.org/10.1038/ncb433